Secondary electron emission in extreme-UV detectors: Application to diamond based devices

I. Ciancaglioni, Marco Marinelli, E. Milani, G. Prestopino, C. Verona et al.

Citation: J. Appl. Phys. **110**, 014501 (2011); doi: 10.1063/1.3602125
View online: http://dx.doi.org/10.1063/1.3602125
View Table of Contents: http://jap.aip.org/resource/1/JAPIAU/v110/i1
Published by the American Institute of Physics.

Secondary electron emission in extreme-UV detectors: Application to diamond based devices

I. Ciancaglioni,[1] Marco Marinelli,[1] E. Milani,[1] G. Prestopino,[2] C. Verona,[1,a)]
G. Verona-Rinati,[1] M. Angelone,[2] and M. Pillon[2]
[1]*Dip. di Ing. Meccanica, Università di Roma "Tor Vergata," Rome, Italy*
[2]*Associazione EURATOM-ENEA sulla Fusione, Frascati (Rome), Italy*

(Received 21 October 2010; accepted 21 May 2011; published online 5 July 2011)

A study on the effect of secondary electron emission, which strongly affects the detection of extreme-UV radiation, was performed on diamond detectors. Two different structures were compared: interdigitated contacts and a transverse Schottky diode configuration. Both devices were electrically characterized by I-V measurements and their responsivity was measured in the extreme UV spectral region (20–120 nm) by using He-Ne gas discharge radiation sources and a toroidal grating vacuum monochromator. Through an ad-hoc measurement configuration, the contributions of the internal photocurrent and of the photoemission current have been analyzed and separately evaluated. The results showed that secondary electron emission, which clearly depends on the experimental conditions (e.g., external electric field, pressure, etc.), is one of the most relevant processes affecting the spectral responsivity in the extreme UV band. In particular, for interdigitated devices, extreme care must be taken in order to obtain an absolute value of their responsivity, while detectors in the transverse configuration can be shielded in such a way to avoid secondary electron current contribution and therefore provide a more correct and reliable response.
 [doi:10.1063/1.3602125]

I. INTRODUCTION

Diamond is a semiconducting material with extreme optical and electronic properties. A wide bandgap, high thermal conductivity, high resistivity, high carrier mobility, and a remarkable radiation hardness[1–3] suggest diamond as an ideal material for electronic devices and, in particular, for the fabrication of highly sensitive solar-blind deep UV photodetectors.[4] Several attempts have been made so far to build up UV and soft x-ray detectors from natural or synthetic diamonds.[5,6] However, detector grade natural diamonds are extremely rare and expensive, high-pressure high-temperature (HPHT) diamonds contain too many impurities, and polycrystalline chemical vapor deposition (CVD) diamonds have poor response times and spatial homogeneity.[7,8] A great amount of effort is therefore being devoted to produce device-grade single crystal diamond films (SCD) by homoepitaxial CVD growth on low-cost diamond substrates.[9,10]

Various photodetector structures based on single crystal CVD diamond, such as a photoconductors with interdigitated electrodes and photodiodes, are reported in the literature.[11,12]

The approach, recently developed at Rome "Tor Vergata" University, consists of using Schottky diodes operating in the photovoltaic regime based on CVD single crystal diamond. Two such devices are permanently installed at the Joint European Torus (JET) fusion reactor to measure UV and soft x-ray radiation produced by the JET plasma demonstrating fast response time, high stability, high discrimination power between UV emission and background radiation (i.e., γ-rays, neutrons and visible light), and good sensitivity.[13]

In a typical vacuum-UV (VUV)/extreme-UV (EUV) measurement, however, the photodetector sensitivity can be affected by the unpredictable contribution arising from secondary electron emission.[14,15] The resulting additional current can significantly contribute to the measured one. It is unstable and can depend on the experimental set-up and environmental conditions, such as the presence of external electric fields, charging effects of the material surrounding the device, atmosphere pressure, etc. This leads to poor reproducibility of the detector response, making a reliable absolute calibration difficult.

In this work, a detailed analysis of the effect of the secondary electron current on EUV measurements is reported by comparing the response of two different photodetector structures in the wavelength range from 20 to 120 nm. Both devices are based on synthetic SCD films produced in our laboratories. The first one is a Schottky diode in a multilayered p-type diamond/intrinsic diamond/Schottky metal configuration with a semitransparent top electrode operating in a transverse configuration. The second configuration, widely reported in the literature, is a photoconductive detector based on a nominally identical single crystal CVD diamond film, having interdigitated electrodes and operating in a planar configuration.

II. EXPERIMENTAL SET-UP

The first diamond detector was built in a multilayered structure obtained by a three step deposition process.

a)Electronic mail: claudio.verona@uniroma2.it.

A highly conductive homoepitaxial boron-doped diamond layer was deposited by microwave plasma-enhanced CVD on a $4 \times 4 \times 0.5$ mm^3 HPHT-type Ib single crystal diamond substrate. Such a p-doped layer was used as a back contact and its resistivity is approximately 0.16 Ω cm. A nominally intrinsic diamond layer was then grown on the doped one and used as the sensitive/active layer. The thickness of the intrinsic layer was chosen to be approximately 2 μm, which is sufficient to completely stop the incident radiation in the $\lambda = 10$–200 nm range.[16] The intrinsic layer was deposited by using a separate CVD reactor in order to avoid any boron contamination. The hydrogen termination of the as-grown surface was removed by isothermal annealing at 500 °C for 1 h in air. Finally, a semitransparent platinum (Pt) top electrode (3 mm in diameter) was deposited on the intrinsic diamond surface by thermal evaporation. Annealed silver paint was used to provide an ohmic contact to the B-doped layer. Such a structure acts as a p-doped/intrinsic diamond/metal (PIM) Schottky barrier diode,[17] producing a built-in potential so that a photovoltaic regime operation is possible with no need for an external applied voltage.

Two different thicknesses of the Pt contact were employed: (i) a thickness of about 5 nm (a minimum of transmission of about 0.5 at $\lambda = 60$ nm) and (ii) a thickness of about 50 nm (transmission < 0.01 in the whole $\lambda = 20$–120 nm examined range).[18] In the latter case the UV light is completely blocked and the contribution to the output current arising from the metallic contact can be measured.

The second diamond detector was fabricated in a planar interdigitated electrode configuration. A 30 μm thick CVD diamond layer was grown on a HPHT single crystal diamond substrate. Aluminum (Al) fingers were then patterned by a standard lift-off photo-lithographic technique and by thermal evaporation. In this case, annealing in air was also performed before the contact deposition in order to remove the surface conductive layer from the as-grown SCD film. Both the width of the fingers and the gap between them are 20 μm. The total optical detection area was approximately 5 mm^2. Such a structure acts as a two-terminal metal-diamond-metal (MDM) device.

The two detectors were tested over the extreme UV spectral region from 20 to 120 nm by using He–Ne dc gas discharge as a radiation source and a toroidal grating vacuum monochromator (Jobin Yvon model LHT-30) with a 5 Å wavelength resolution. The size of the optical aperture was 0.25×6.00 mm^2 and a manual shutter was used to switch the UV radiation on and off. Using a three-dimension (X–Y–Z) mechanical stage powered by stepper motors, it was possible to locate the photodetector in front of the beam light and to compare its response with that of a calibrated NIST silicon photodiode[19] placed in the same position.

The photoemission current (I_e, in the following text) was separately measeured from the internally generated photocurrent (I_{ph}, in the following text) by using two electrometers and a voltage source to change the bias voltage applied to a copper/vetronite shielded housing with a 2 mm pinhole that collimates the impinging radiation beam on the sensitive area of the diamond detectors. Moreover, the PIM detector was encapsulated by using silicone to isolate the p-type diamond contact from the top metallic electrode. A schematic of the electrical measurement setup is shown in Fig. 1.

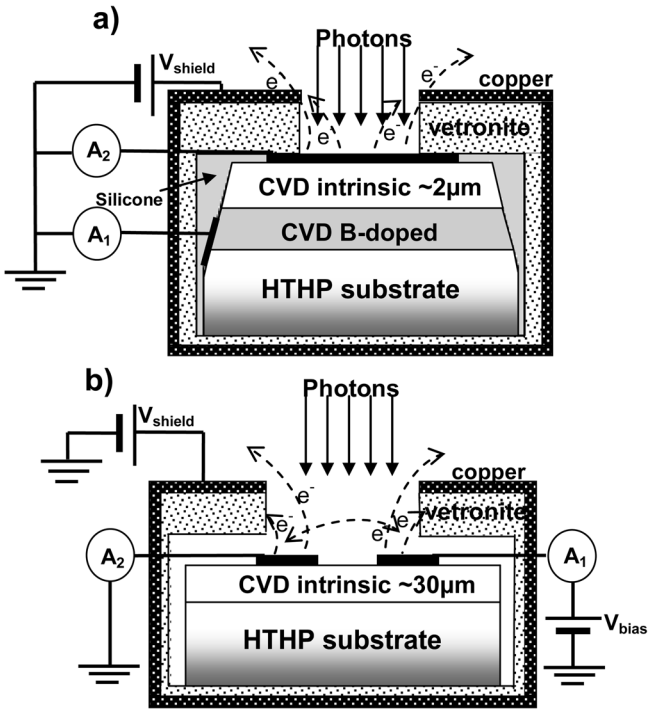

FIG. 1. Schematic representation of measurement configuration and of the investigated devices: (a) p-type/intrinsic diamond/metal Schottky photodiodes, and (b) photoconductive detector operating in planar configuration with Al interdigitated electrodes.

The photocurrents were measured by a Keithley 6517 A picoammeter and a Keithley 2001 multimeter with a low noise FEMTO transimpedance amplifier as front-end electronics. The internal voltage source of the Keithley 6517 A was used as the bias voltage for both devices.

As shown in Fig. 1(a) the electrometer, A_1, measures the positive internal photocurrent, I_{ph}, of the device flowing from the top Pt electrode to the p-type SCD. The current measured by electrometer, A_2, can instead contain both the photoemission current and the internally generated current, depending on the bias voltage applied to the metallic shield (V_{shield}). In particular, when V_{shield} is sufficiently high, the photo-emitted electrons are collected by the shield so that the positive photoemission current, I_e, is superimposed to the negative contribution, I_{ph}, measured by A_2. The currents measured by the two electrometers are therefore given by,

$$\begin{aligned} I_{A_1} &= I_{ph}, \\ I_{A_2} &= I_e - I_{ph}. \end{aligned} \tag{1}$$

On the contrary, when the voltage applied to the metallic shield is negative, the photoemitted electrons give no contribution to the measure current. Hence, in this case the only internal photocurrent is detected by both electrometers.

In the MDM photoconductive detector shown in Fig. 1(b), the situation is more complicated. In the first approximation, if $|V_{shield}| \gg |V_{bias}|$, neglecting the fraction of photoemitted electrons collected directly by the

interdigitated contacts (likely due to their proximity) and that emitted by the irradiated oxidized diamond surface, i.e., considering only the secondary electrons coming out of the metallic contacts (I_{e1}, I_{e2}), when a positive voltage is applied to the detector ($V_{bias} > 0$) the currents measured by the two electrometers are,

$$\begin{aligned} I_{A_1} &= -I_{ph} + I_{e_1}, \\ I_{A_2} &= I_{ph} + I_{e_2}. \end{aligned} \tag{2}$$

Clearly, if $V_{bias} < 0$, the sign of the photoconductive current measured by two electrometers is reversed. A positive sign is assumed in Eqs. (1) and (2) for the currents flowing from the device to ground.

With the aid of Eqs. (1) and (2), the I_{ph} contribution can be isolated, which we will discuss in the next section.

III. RESULTS AND DISCUSSION

The results obtained by the two photodetectors are separately reported in the following text. In particular, the effect of the photoemission current is analyzed and its contribution to the device responsivity is evaluated in both cases.

A. Transverse configuration

In Fig. 2, the current versus voltage (I-V) characteristics of the PIM detector are reported. Measurements have been performed at room temperature in a vacuum chamber, both in the dark condition and under broadband UV irradiation (the monochromator grating positioned at the zero order reflection). A rectification ratio of about 10^9 at ± 3 V and a dark current lower than 150 fA for reverse bias voltages below 8 V ($\sim$4 V/μm) were observed. The detector shows a photocurrent response even at zero voltage bias, due to the built-in potential at the top electrode–intrinsic diamond interface. The best signal-to-dark current ratio is obtained at zero bias so that the device was tested with no external bias voltage applied.

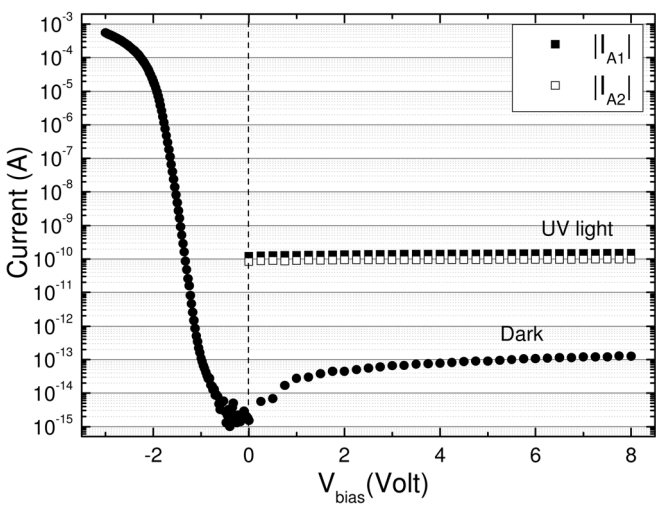

FIG. 2. I-V characteristics in the dark and under broadband UV irradiation of the PIM detector. The photocurrents are measured by the two electrometers, A_1 and A_2.

From the data reported in Fig. 2, it is shown that the photocurrents measured by the two electrometers are different. In particular, the photocurrent measured by electrometer, A_1, is about a factor of 1.5 higher than that measured by A_2. This effect can be explained by the presence of the photoemission current, which is significant in the extreme UV spectral region.

To better understand the photoemission contribution to the measured current, the applied voltage, V_{shield}, was changed in order to attract or repel the photo-emitted electrons which originated at the irradiated device surface. The current versus time plot measured by the two electrometers with $V_{shield} = +100$ V and -100 V is shown in Fig. 3. As expected from Eq. (1), the current measured by electrometer, A_2, drops with respect to the $V_{shield} = 0$ V case when V_{shield} is $+100$ V, because the photo-emitted electrons are extracted more effectively from the illuminated detector surface [Fig. 3(a)]. On the contrary, for $V_{shield} = -100$ V, the photo-emission current is completely blocked by the electric field produced by the shield and the currents measured by the two electrometers are nearly identical [Fig. 3(b)]. The current measured by electrometer, A_1, does not change with V_{shield}, demonstrating that the only internal photocurrent generated in the intrinsic SCD layer of the PIM detector is measured by A_1.

For a more detailed analysis, the currents measured by the two electrometers at $\lambda = 30.4$ nm (He line) and $\lambda = 74$ nm (Ne line) are reported in Fig. 4(a) as a function of V_{shield} in the case of a 5 nm thick top Pt electrode. The current measured by electrometer, A_1, at both wavelengths is the same for all voltages applied to the shield, whereas the one measured by electrometer, A_2, strongly depends on V_{shield} at $\lambda = 74$ nm. In this latter case, the photocurrent measured by electrometer, A_2, changes sign when a voltage higher than $+15$ V is applied to the shield, demonstrating a dominant contribution of secondary electrons with respect to the photocurrent at this wavelength. In addition, a clear plateau is observed for $V_{shield} > +50$ V, also indicating a high efficiency of the shield in collecting secondary electrons. The presence of secondary electrons is sensibly lower at $\lambda = 30.4$ nm, since the currents

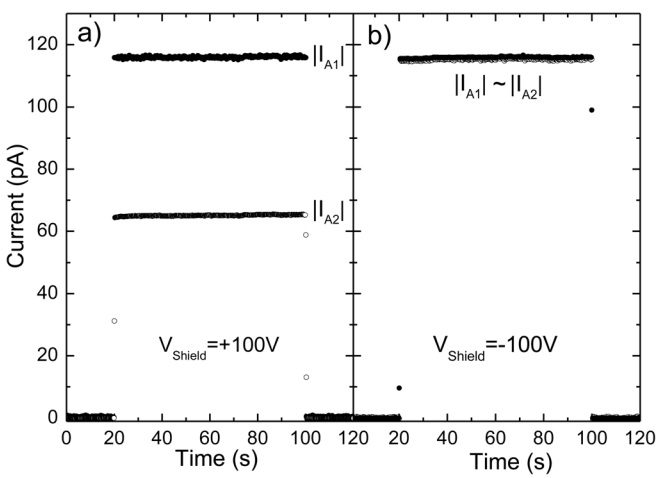

FIG. 3. Time response of the PIM detector measured by the two electrometers with (a) $V_{shield} = +100$ V, and (b) $V_{shield} = -100$ V.

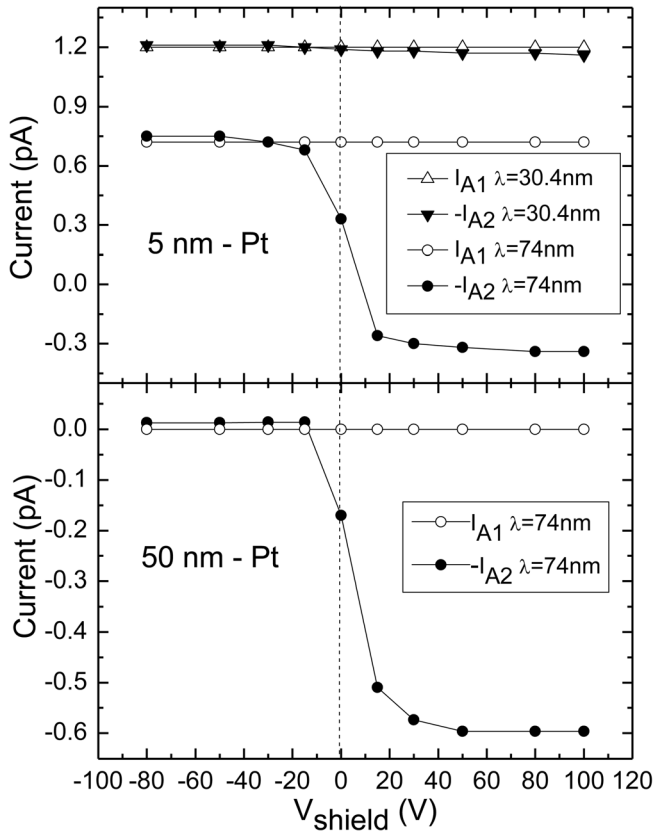

FIG. 4. Currents measured by the two electrometers at $\lambda = 30.4$ nm (He line) and $\lambda = 74$ nm (Ne line) as a function of V_{shield} for (a) 5 nm thick, and (b) 50 nm thick Pt top electrode of the PIM detector.

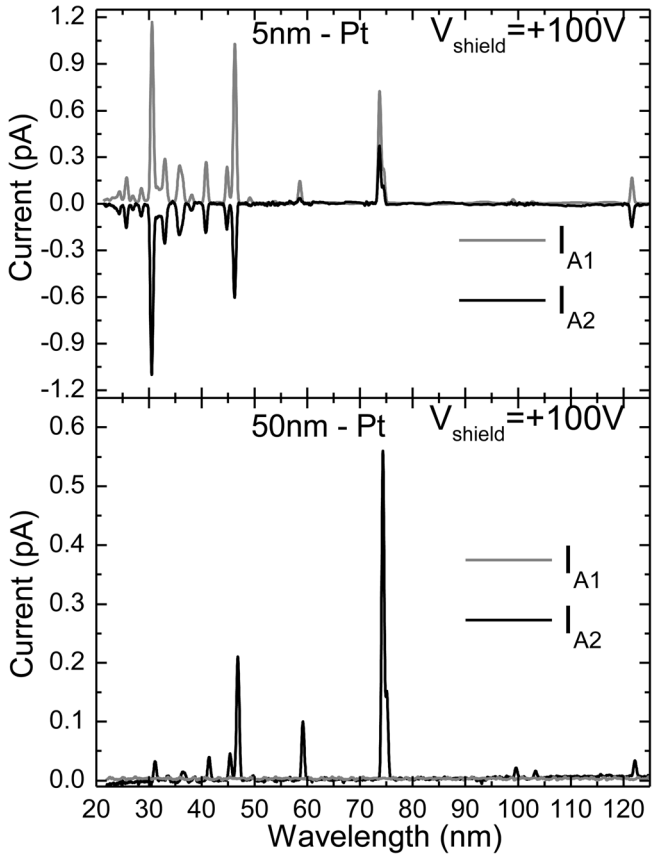

FIG. 5. Emission spectrum of the He-Ne dc gas discharge measured by the PIM detector with $V_{shield} = +100$ V through the two electrometers using: (a) 5 nm thick Pt and (b) 50 nm thick Pt.

measured by the two electrometers are very similar in the whole investigated V_{shield} voltage range.

In Fig. 4(b) the photocurrents measured at $\lambda = 74$ nm by the two electrometers as a function of V_{shield} using a 50 nm thick Pt contact are shown. The contribution of the secondary electron current at 74 nm is confirmed. In this case, however, the internal photocurrent measured by electrometer, A_1, is always zero because the thick Pt contact totally cuts off the UV irradiation. The current measured by electrometer, A_2, is thus given only by secondary electrons arising from the metal top electrode.

The emission spectrum of the He-Ne dc gas discharge, as measured by the PIM detector in unbiased mode with $V_{shield} = +100$ V, is reported in Fig. 5. All of the spectral lines of the He-Ne gas are clearly resolved and measured with a good signal to noise ratio, demonstrating the photodetection capabilities of the PIM photodetector in the extreme UV spectral region. The spectral lines measured by the two electrometers are almost identical in amplitude at the shortest ($\lambda < 50$ nm) and longest ($\lambda > 100$ nm) wavelengths. A change of sign of the signal measured by electrometer, A_2, can be observed from 50 to 100 nm, indicating a large increase of the photo-emission contribution at intermediate wavelengths.

To verify such a hypothesis, only the spectrum of the photoemission current (obtained using the 50 nm thick Pt electrode) is reported in Fig. 5(b). The peak amplitudes in this spectrum account for the differences observed in Fig. 5(a).

From the measured spectra, it is possible to calculate the absolute spectral response, *R*, of the PIM detector, defined as the total current per unit incident power, by comparison with a calibrated silicon photodiode exposed to the same source on the same optical area. The responsivity curves as measured by the two electrometers with $V_{shield} = +100$ V are shown in Fig. 6. The value of the responsivity, R_{A1}, measured by electrometer, A_1 (i.e., the internal photocurrent) increases toward the edges of the investigated spectral range

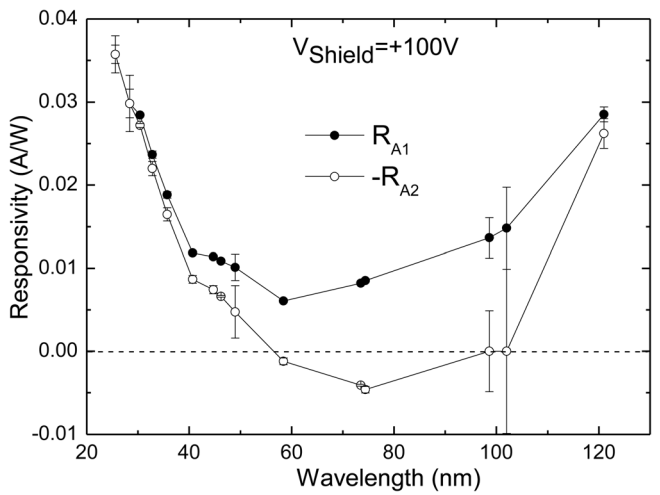

FIG. 6. Responsivity curves of the PIM detector measured by the two electrometers with $V_{shield} = +100$ V.

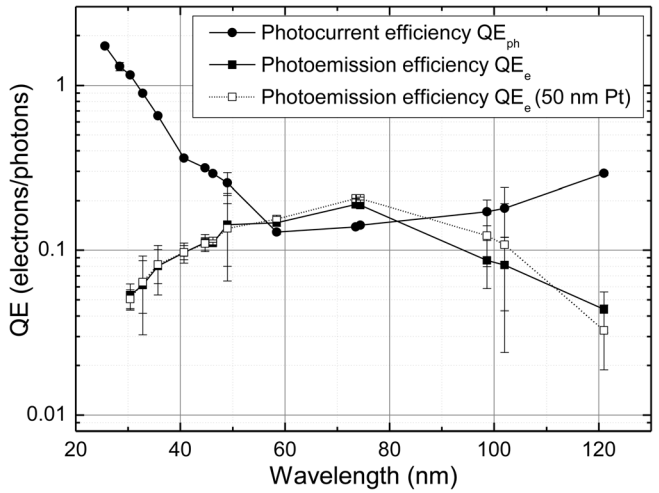

FIG. 7. Internal photocurrent efficiency (QE_{ph}) and the photoemission quantum efficiency (QE_e) of the PIM detector in the range of 20–120 nm.

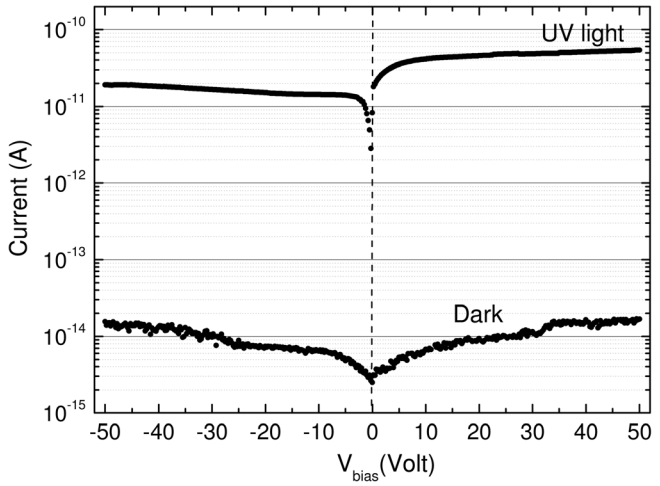

FIG. 8. The I-V characteristics in the dark and under broadband UV for the MDM photoconductor.

and presents a deep minimum for intermediate wavelengths at about 60 nm. As previously mentioned, such wavelengths correspond to the minimum value of the transmission coefficient of the Pt layer. On the contrary, the responsivity, R_{A2}, measured by electrometer, A_2 ($-R_{A2}$ in Fig. 6) is negative at the extreme wavelengths [$|I_{ph}| > |I_e|$; see Eq. (1)] and positive at the intermediate ones, due to the secondary electron contribution, which is found to be dominant in this spectral range ($|I_e| > |I_{ph}|$).

The quantum efficiency, defined by the number of photoelectrons per incident photons is given by $QE = R \times hc/\lambda e$. According to Eq.(1), the secondary electron emission efficiency, $QE_e = (R_{A1} + R_{A2})hc/\lambda e$, can be derived. The calculated data are reported in Fig. 7 (filled squares).

The electron emission efficiency was also directly measured through the A_2 electrometer using a 50 nm thick Pt contact on the PIM detector. The corresponding values (open squares in Fig. 7) are in agreement with those indirectly obtained from the detector with the thin Pt contact. It can be see that the contribution of the photoemission current to the total output current is not negligible and shows a maximum intensity of about 0.2 electrons/photons at around 74 nm. These observations are in agreement with the photoelectron yield of metals reported in the literature.[20–22] In Fig. 7, the internal photocurrent efficiency, QE_{ph}, is also reported (filled circles). It can be seen that QE_{ph} is higher than unity at low wavelengths. This is because at such photon energies, multiple ionizations are energetically possible so that more than one electron–hole pair can be generated per incident photon.

B. Planar configuration

The I-V characteristics in the dark and under broadband UV irradiation are shown in Fig. 8 for the MDM photoconductor. The measurement was performed in vacuum using a single electrometer in a standard high resistance connection configuration, i.e., connecting the ammeter to one contact of the device and the voltage source terminal to the opposite contact.[23] The dark current is very low ($\sim 10^{-14}$ A) in the ± 50 V voltage range. The photocurrent shows a sharp initial increase with bias voltage and tends to saturate as V_{bias} increases. Note that, in principle, due to the symmetric geometry of the device, a symmetric I-V curve would be expected.

This is actually observed for the dark current but a large difference is visible in Fig. 8 between positive and negative bias polarity under UV irradiation. This asymmetry can be explained by considering the contribution of the secondary electrons arising from the metallic interdigitated contacts. In fact, as expected from Eq. (2), when $V_{bias} > 0$ V the contribution of secondary electrons is added to the photocurrent whereas, if $V_{bias} < 0$ V, this contribution is subtracted.

The I-V curves under broadband UV irradiation (74 and 30.4 nm) were measured in order to verify such an explanation. The results are reported in Fig. 9 (filled circles). The same measurements were repeated after interchanging the two terminals of the device and are also reported in Fig. 9 (open circles).

A good overlap between each I-V characteristic and its corresponding curve with the interchanged connection was observed, demonstrating the symmetric transport properties of such a device. In addition, the asymmetry of the I-V curve with respect to V_{bias} polarity is observed to be much more pronounced at $\lambda = 74$ nm than at $\lambda = 30.4$ nm, being the photoelectric contribution more relevant at the former wavelength, as shown in the transverse configuration case.

This result shows that, despite the device symmetry, it is important to specify the polarity of the applied voltage to the detector and the position of the ammeter in the connection circuit, since the photoemission contribution may strongly affect the device response.

Similar to the transverse configuration case discussed in the previous section, in order to discriminate the secondary electron contribution, voltage was applied to the shield surrounding the detector [see Fig. 1(b)]. The currents measured by the two electrometers, A_1 and A_2, as a function of V_{shield} when the device is exposed to 30.4 and 74 nm wavelengths, are reported in Fig. 10. Two different bias voltages, +30 V [Fig. 10(a)] and −30 V [Fig. 10(b)], were considered.

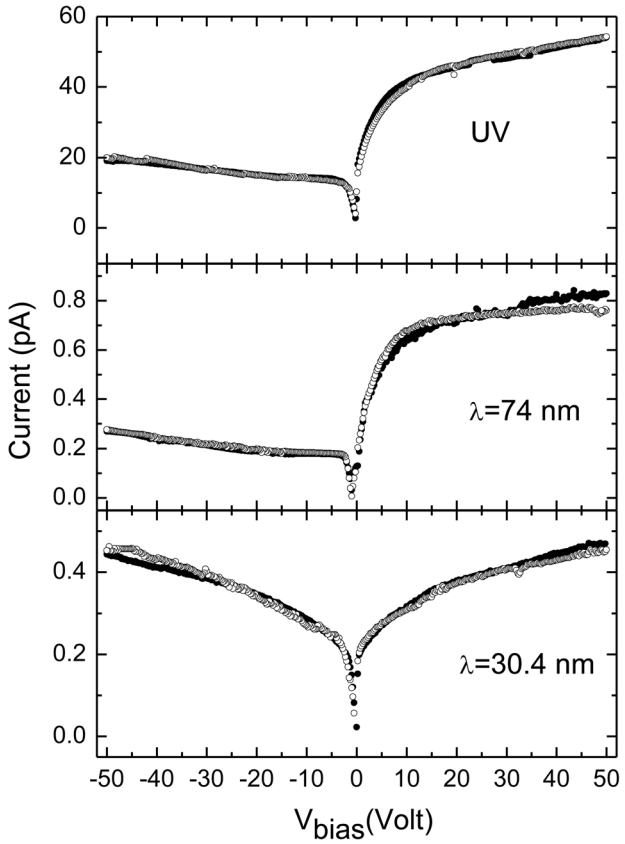

FIG. 9. I-V curves under broadband UV irradiation, 74 and 30.4 nm (filled circles). Measurements are reported after interchanging the two terminals of the MDM device (open circles).

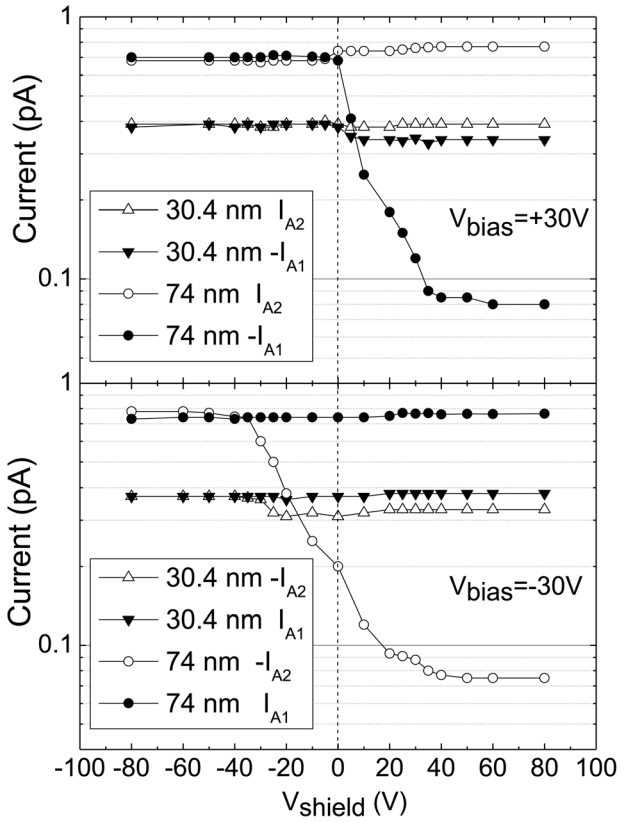

FIG. 10. Currents measured by the two electrometers, A_1 and A_2, as a function of V_{shield} when the MDM device is exposed to 30.4 and 74 nm wavelengths with (a) +30 V and (b) −30 V bias voltages.

At $V_{bias} = +30$ V, for negative shield potentials, very similar currents are measured by the two ammeters. This is because the secondary electrons, repelled by the shield, are attracted toward the electrode with the highest potential so that almost all of the electrons emitted by one electrode are collected by the other one, producing an equal contribution to the measured currents by the two ammeters.

When high positive voltages are applied to the shield, current plateaus are observed with a high discrepancy between the two ammeters, especially at the 74 nm wavelength where a much more pronounced electron emission is present. This behavior can be explained by considering that practically all of the photoelectrons are collected by the shield and the current of the secondary electrons between the electrodes can be neglected. In this assumption, for $V_{bias} = +30$ V [Fig. 10(a)], the currents, I_{A1} and I_{A2}, are given by Eq. (2).

It is interesting to note that I_{A2} does not change significantly with the shield polarity because the corresponding electrode emits electrons independently by the shield potential: for negative V_{shield} the photoelectrons are emitted toward the opposite electrode (higher potential), while for positive values of V_{shield} the electrons are emitted toward the shield. The current I_{A2} is thus given in both cases by the sum of the photocurrent and of the photoelectron current. On the contrary, I_{A1} decreases its absolute value by increasing the shield potential because for a negative value of V_{shield} its corresponding electrode collects electrons emitted by the opposite contact and for large positive shield potentials it emits photoelectrons toward the shield.

For $V_{bias} = -30$ V [Fig. 10(b)], the system works similarly to the previous case, but the photocurrent changes its direction so that now it has the same sign of the photoemission current in the ammeter, A_1, and the opposite sign in A_2. In particular, by considering the relative potentials between the contacts and the shield, it can be seen that the electronic conditions at $V_{bias} = -30$ V are equivalent to the previous ones after a −30 V shift of all the potentials with interchanged electrometers. This behavior is experimentally observed and it is clearly visible by comparing Figs. 10(a) and 10(b).

The results shown in Fig. 10 demonstrate that for a high positive shield potential it is possible to separate the photocurrent and photoemission contribution to the detector signal. Assuming that the secondary electron currents from the two electrodes are approximately equal [$I_{e1} = I_{e2}$ in Eq. (2)], for positive V_{bias} we obtain the following equations from Eq. (2),

$$I_{ph} = \frac{I_{A2} - I_{A1}}{2}, \qquad I_e = \frac{I_{A1} + I_{A2}}{2}. \tag{3}$$

A similar relation can be obtained for negative V_{bias}.

We found that the photoemission contribution to the total signal ($I_{ph} + I_e$) is about 45 and 7% at the 74 and 30.4 nm wavelengths, respectively. This result is expected to be specimen dependent since the photoemission current

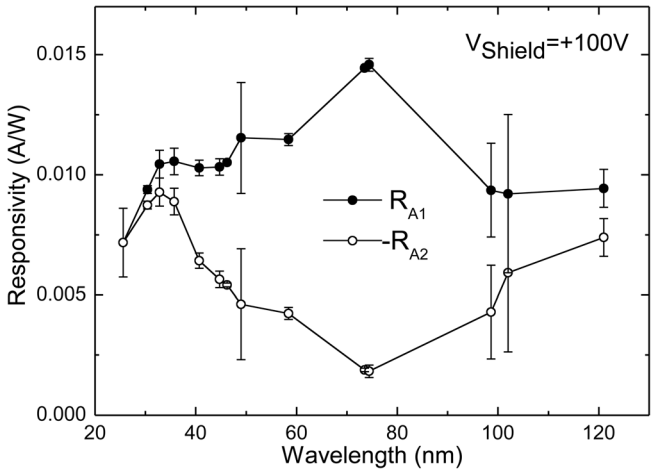

FIG. 11. Responsivity of the MDM detector measured by the two electrometers with $V_{shield} = +100$ V and $V_{bias} = 50$ V.

depends on several factors such as the metal contact, surface condition, etc.[24–26]

In order to obtain the contribution of the photocurrent and photoemission current over the whole investigated spectral region, the emission spectrum of the He-Ne discharge in the 20–120 nm wavelength range was measured by the MDM photoconductor. The responsivities measured by the two electrometers, R_{A1} and R_{A2}, with $V_{shield} = +100$ V and $V_{bias} = 50$ V were then calculated and reported in Fig. 11.

The differences between the responsivities measured by the two electrometers are ascribed to the wavelength-dependent contribution of secondary electron photoemission in the investigated spectral range. In particular, considering their absolute values, the measured currents are similar toward the edges of the investigated wavelength range while a large difference is observed at intermediate wavelengths.

The currents of both the photoconductive and photoemission components were then separately calculated from the data reported in Fig. 11 by using Eq. (3). The corresponding quantum efficiencies are reported in Fig. 12.

The quantum efficiency, QE_{ph}, of the internal photocurrent, I_{ph}, decreases almost monotonically from 0.3 to 0.1 electrons/photons in the wavelength range from 30 to 100 nm, whereas the quantum efficiency, EQ_e, of the photoemission current contribution, I_e, has a maximum efficiency of 0.1 electrons/photons at about 74 nm and rapidly decreases toward the edge of the investigated region.

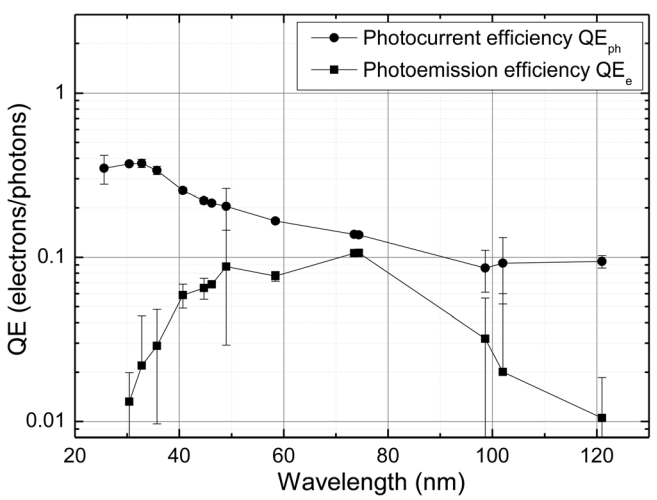

FIG. 12. Internal photocurrent efficiency (QE_{ph}) and the photoemission quantum efficiency (QE_e) of the MDM detector in the range of 20–120 nm.

Comparing the results obtained by the two tested device configurations, it can be seen that the internal photocurrent of the two detectors are similar at intermediate wavelengths (50–100 nm) while a much larger photocurrent efficiency of the detector operating in the transverse configuration is observed toward the extremes of the investigated wavelength range. Such a different behavior could be qualitatively ascribed to the different geometries of the tested devices. In particular, the active surface of the MDM device is lower than the exposed one, being the diamond surface partially covered by the interdigitated contacts. This is not the case for the PIM device where a semitransparent electrode is used. Therefore, the PIM device generally shows a higher efficiency but presents an absorption band at an intermediate wavelength, mainly due to the presence of the Pt contact at the surface.

IV. CONCLUSIONS

A study on the effect of secondary electron emission on the detection properties of the extreme UV diamond detectors have been performed. Two different detector structures were analyzed: interdigitated contact and the transverse Schottky diode configuration. The contributions of the internal photocurrent and the photoemission current have been shown and separately evaluated. The photoemission current contribution to the total output current is not negligible and even dominant at wavelengths between 50 and 100 nm. Moreover, the internal photocurrent generated in the detector operating in the transverse configuration is larger than that generated in a device with planar interdigitated electrodes for all of the investigated wavelengths, except for 60 nm.

In the case of the planar configuration, the signal is directly collected from the interdigitated electrode on the irradiated surface and therefore, the measured photocurrent contains both photoconductive current and photoemission current. The latter can depend on the operative condition surrounding the photodetector (e.g., external electric field, pressure, etc.). Extreme care must be taken when measuring the responsivity of such planar detectors, and absolutely calibrating their response.

On the contrary, in the transverse configuration, with an appropriate experimental set-up, the photocurrent measured between the p-type diamond electrode and ground is not affected by the presence of the secondary electron emission current from the illuminated contact. Therefore, the detector responsivity does not depend upon the set-up conditions and a reliable absolute calibration of such devices can be performed.

[1]J. E. Field, *Properties of Diamond* (Academic, London, 1979).
[2]J. Prins, "Applications of diamond films in electronics," in *The Physics of Diamond*, edited by A. Paoletti and A. Tucciarone (IOS, Amsterdam, 1997).
[3]M. Pillon, M. Angelone, G. Aielli, S. Almaviva, M. Marinelli, E. Milani, G. Prestopino, A. Tucciarone, C. Verona, and G. Verona-Rinati, J. Appl. Phys. **104**, 054513 (2008).

[4]J.-F. Hochedez, J. Alvarez, F. D. Auret, P. Bergonzo, M.-C. Castex, A. Deneuville, J. M. Defise, B. Fleck, P. Gibart, S. A. Goodman, O. Hainaut, J.-P. Kleider, P. Lemaire, J. Manca, E. Monroy, E. Munoz, P. Muret, M. Nesladek, F. Omnes, E. Pace, J. L. Pau, V. Ralchenko, J. Roggen, U. Schuhle, and C. Van Hoof, Diamond and Relat. Mater. **11**, 427 (2002).
[5]E. V Gorokhov, A. N. Magunov, V. S. Feshchenko and A. A. Altvkhov, Instrum. Exp. Tech. **51**, 280 (2008).
[6]Y. Iwakaji, M. Kanasugi, O. Maida and T. Ito, Appl. Phys. Lett. **94**, 223511 (2009).
[7]L. Barberini, S. Cadeddu, and M. Caria, Nucl. Instrum. Methods Phys. Res. A **460**, 127 (2001).
[8]R. D. McKeag and R. B. Jackman, Diamond Relat. Mater. **7**, 513 (1998).
[9]T. Teraji, S. Yoshizaki, H. Wada, M. Hamada, and T. Ito, Diamond Relat. Mater. **13**, 858 (2004).
[10]J. H. Kaneko, T. Teraji, Y. Hirai, M. Shiraishi, S. Kawamura, S. Yoshizaki, T. Ito, K. Ochiai, T. Nishitani, and T. Sawamura, Rev. Sci. Instrum. **75**, 358 (2004).
[11]M. Liao, Y. Koide, and J. Alvarez, Appl. Phys. Lett. **88**, 33504 (2006).
[12]A. BenMoussa, A. Soltani, K. Haenen, U. Kroth, V. Mortet, H. A. Barkad, D. Bolsee, C. Hermans, M. Richter, J. C. De Jaeger, and J. F. Hochedez, Semicond. Sci. Technol. **23**, 035026 (2008).
[13]M. Pillon, M. Angelone, M. Marinelli, E. Milani, G. Prestopino, C. Verona, G. Verona Rinati, I. Coffey, A. Murari, and N. Tartoni, Nucl. Instrum. Methods Phys. Res. A **623**, 726 (2010).
[14]T. Saito and K. Hayashi, Appl. Phys. Lett. **86**, 122113 (2005).
[15]T. Saito, Metrologia **40**, 159 (2003).
[16]D. Palik, *Handbook of Optical Constants of Solids II* (Academic, New York, 1991).
[17]S. Almaviva, M. Marinelli, E. Milani, G. Prestopino, A. Tucciarone, C. Verona, G. Verona-Rinati, M. Angelone, M. Pillon, I. Dolbnya, K. Sawhney, and N. Tartoni, J. Appl. Phys. **107**, 014511 (2010).
[18]See: http://henke.lbl.gov/optical_constants/filter2.html. for x-ray optical transmission data for elements.
[19]See: http://www.ird-inc.com. International Radiation Detectors (IRD).
[20]W. Pong, R. Sumida, and G. Moore, J. Appl. Phys. **41**, 1869 (1970).
[21]S. F. Lin, D. T. Pierce, and W. E. Spicer, Phys. Rev. B **4**, 326 (1971).
[22]J. J. Yeh and I. Lindau, At. Data Nucl. Data Tables **32**, 1 (1985).
[23]See: Keithley Model 6517A Electrometer User's Manual: http://www3.imperial.ac.uk/pls/portallive/docs/1/7293199.PDF.
[24]J. Ristein, W. Stein, and L. Ley, Diamond and Relat. Mater. **7**, 626 (1998).
[25]W. Pong, R. Sumida, and G. Moore, J. Appl. Phys. **41**, 1869 (1970).
[26]M. C. Rossi, F. Spaziani, G. Conte, and V. Ralchenko, Diamond and Relat. Mater. **14**, 552 (2005).